On the Production Behavior of Enhanced Geothermal Systems with CO_2 as Working Fluid

Karsten Pruess

Earth Sciences Division, Lawrence Berkeley National Laboratory

University of California, Berkeley, CA 94720

K_Pruess@lbl.gov

Abstract

Numerical simulation is used to evaluate mass flow and heat extraction rates from enhanced geothermal injection-production systems that are operated using either CO_2 or water as heat transmission fluid. For a model system patterned after the European hot dry rock experiment at Soultz, we find significantly greater heat extraction rates for CO_2 as compared to water. The strong dependence of CO_2 mobility (= density/viscosity) upon temperature and pressure may lead to unusual production behavior, where heat extraction rates can actually increase for a time, even as the reservoir is subject to thermal depletion. We present the first-ever three-dimensional simulations of CO_2 injection-production systems. These show strong effects of gravity on mass flow and heat extraction, due to the large contrast of CO_2 density between cold injection and hot production conditions. The tendency for preferential flow of cold, dense CO_2 along the reservoir bottom can lead to premature thermal breakthrough. The problem can be avoided by producing from only a limited depth interval at the top of the reservoir.

Keywords: enhanced geothermal systems (EGS), heat transmission, thermal breakthrough, CO_2 storage, numerical simulation.

Introduction

A novel concept for operating enhanced geothermal systems (EGS) with high pressure (supercritical) CO_2 instead of water as heat transmission fluid was proposed by D. Brown [1]. As pointed out by Brown, CO_2 has certain thermophysical and chemical properties that could make it attractive as a heat transfer medium. Water losses present a serious obstacle to commercialization of water-based EGS [2], while fluid losses in an EGS operated with CO_2 could achieve geologic storage of CO_2 as an ancillary benefit. An additional motivating factor for exploring CO_2 as working fluid is that water-based EGS face significant technical difficulties from mineral dissolution and precipitation, due to strong chemical interactions between rocks and aqueous fluids at geothermal temperatures [3-7]. These give rise to the twin problems of short-circuiting flow paths from injector to producer with premature thermal breakthrough on the one hand, formation plugging on the other. CO_2 is not an ionic solvent, and no significant dissolution-precipitation problems would be expected in the "core" of an EGS operated with CO_2, where all aqueous phase has been removed by dissolution into the flowing CO_2 stream [8]. Table 1 shows a summary comparison of CO_2 and water for use as working fluids in EGS; properties considered favorable are shown bold-faced.

Table 1. Comparing CO_2 and water as heat transmission fluids for EGS. Favorable properties are shown bold-faced.

fluid property	CO_2	water
chemistry	**not an ionic solvent; poor solvent for rock minerals**	powerful solvent for rock minerals: lots of potential for dissolution and precipitation
fluid circulation in wellbores	**large compressibility and expansivity** **==> more buoyancy, lower parasitic power consumption to maintain circulation**	small compressibility, moderate expansivity ==> less buoyancy; substantial power requirements for pumps to keep fluids circulating
ease of flow in reservoir	**lower viscosity**, lower density	higher viscosity, **higher density**
heat transmission	smaller specific heat	**larger specific heat**
fluid losses	**may earn credits for storing greenhouse gases**	costly, obstacle to reservoir development

A first quantitative exploration of the heat extraction and mass flow behavior of EGS operated with CO_2 was reported in [9]. Simulation studies for a hypothetical fractured reservoir patterned after the Soultz system in eastern France [10, 11] showed approximately 50 % larger heat extraction rates for CO_2 as compared to water for a reservoir temperature of 200 ^{o}C, with the

advantage of CO_2 increasing for lower reservoir temperature. These observations were explained in terms of the strong increase of water viscosity with decreasing temperature. For a water-based system, much of the pressure differential between injection and production wells is used up to move the very viscous fluid in the vicinity of the injection well. In contrast, viscosity of CO_2 increases much less with lower temperatures, so that a greater fraction of the applied pressure drop is available at the production well. In addition, CO_2 flow in the low-temperature region surrounding the injection well is facilitated by the substantial density increase of CO_2 with decreasing temperatures.

The simulation studies reported in [9] compared CO_2 and water-based EGS for a limited range of thermodynamic conditions; for example, initial reservoir pressure was specified as 500 bar (1 bar = 10^5 Pa) in all cases. There were other limitations as well, such as the use of a two-dimensional (2-D) areal model for the EGS reservoir. Such a model may be adequate for a water-based system, but for CO_2 the density difference between hot fluid near the production wells and cold fluid near the injectors is much larger than for water, so that significant buoyancy and 3-D flow effects may be expected.

This study focuses on energy production from CO_2-EGS. We first examine production behavior in a 2-D areal model for a broad range of pressure conditions, and subsequently assess 3-D flow effects and their impact on energy recovery from EGS operated with CO_2. Issues of fluid loss and associated CO_2 storage and storage integrity are currently being investigated and will be discussed in a future publication.

Dependence of Flow Behavior on Reservoir Pressure (2-D Reservoir Model)

As in our previous work [9] we consider an idealized fractured reservoir problem with parameters representative of conditions at the European EGS site at Soultz (Table 2). Assuming a five-spot well configuration, the computational grid needs to cover only 1/8 of the domain (see Fig. 1). All simulation results will be scaled and reported on a "full well" basis. We use a two-dimensional parallel five-point grid of 36 square blocks with 70.71 m side length. The reservoir is assumed fractured with three orthogonal fracture sets of 50 m spacing. The top and bottom boundaries are assumed impervious. For the simulations reported in this section we neglect conductive heat exchange with cap and base rocks; this approximation is examined in a separate section, below. The matrix blocks are assumed to have negligible permeability, but will provide the main inventory of thermal energy. Matrix-fracture heat exchange is modeled using the method of "multiple interacting continua" (MINC; [12]), with subgridding of matrix blocks into five continua, for a total of 5x36 = 180 grid blocks. Fluid circulation is established by applying an overpressure of 10 bar at the injection side, and an underpressure of -10 bar at the production side, relative to original reservoir pressure. We monitor produced flow rate F and net heat extraction rate G, calculated as $G = F(h - h_{inj})$, where h is produced specific enthalpy, and h_{inj} is specific enthalpy at injection conditions of $T = 20\ ^{o}C$. All simulations were done with our general-purpose reservoir simulator TOUGH2, augmented with a fluid property module "EOSM" that can describe all phase combinations of water-CO_2 mixtures within experimental accuracy, including pure water and pure (anhydrous) CO_2 in supercritical, liquid, and gaseous conditions [13, 14]. Simulations reported here are either for "CO_2 only" or "water only" systems. Mixtures of CO_2 and water would be encountered during the early (development) phase of an

EGS-CO2, as well as in the periphery of an EGS operated with CO_2 [8], and have not been considered here.

Fig. 2 shows simulated heat extraction rates for an initial reservoir temperature of 200 ^oC and pressures of 500, 200, 100, and 45 bar, respectively. Although in "normal" crustal conditions temperatures approaching 200 ^oC will only be encountered at depths of 5 km or more, such temperatures may be found at shallower depths, corresponding to smaller ambient fluid pressures, in the caprock or margins of hydrothermal systems. Such systems may provide early targets of opportunity for EGS. For comparison, we also simulated heat extraction performance of water-based systems for the same T,P-conditions and reservoir parameters. It turns out that the production behavior of water-based systems is rather insensitive to initial reservoir pressure, and the single curve labeled "water" in Fig. 2 represents the performance of water-based EGS over the entire range of pressures considered. It is seen that heat extraction rates for systems using supercritical CO_2 ($P > P_{crit} = 73.82$ bar) are considerably larger than for water-based systems. For sub-critical CO_2 ($P = 45$ bar) a much lower heat extraction rate is obtained, as was expected due to the much lower density of gaseous as compared to supercritical CO_2. This low-pressure case was included only for completeness; it is not of practical interest and will not be considered further.

Table 2. Parameters for five-spot fractured reservoir reference case.

Formation	
thickness	H = 305 m
fracture spacing	D = 50 m
permeable volume fraction	f = 2%
permeability	$k = 50.0 \times 10^{-15}$ m^2
porosity in permeable domain*	$\phi_f = 50\%$
rock grain density	$\rho_R = 2650$ kg/m^3
rock specific heat	$c_R = 1000$ J/kg/°C
rock thermal conductivity	$\lambda = 2.1$ W/m/°C
Initial Conditions	
reservoir fluid	all CO_2, or all water
temperature	$T_{in} = 200$ °C
pressure	$P_{in} = 45$ - 500 bar
Production/Injection	
pattern area (Fig. 1)	A = 1 km^2
injector-producer distance	L = 707.1 m
injection temperature	$T_{inj} = 20$ °C
injection pressure (downhole)	$P_{inj} = P_{in} + 10$ bar
production pressure (downhole)	$P_{pro} = P_{in} - 10$ bar

* we include some wall rock in the definition of the fracture domain

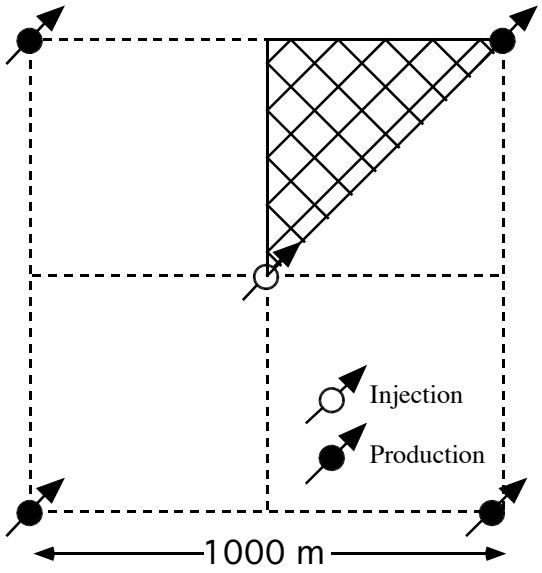

Figure 1. Five-spot well pattern with computational grid for modeling a 1/8 symmetry domain.

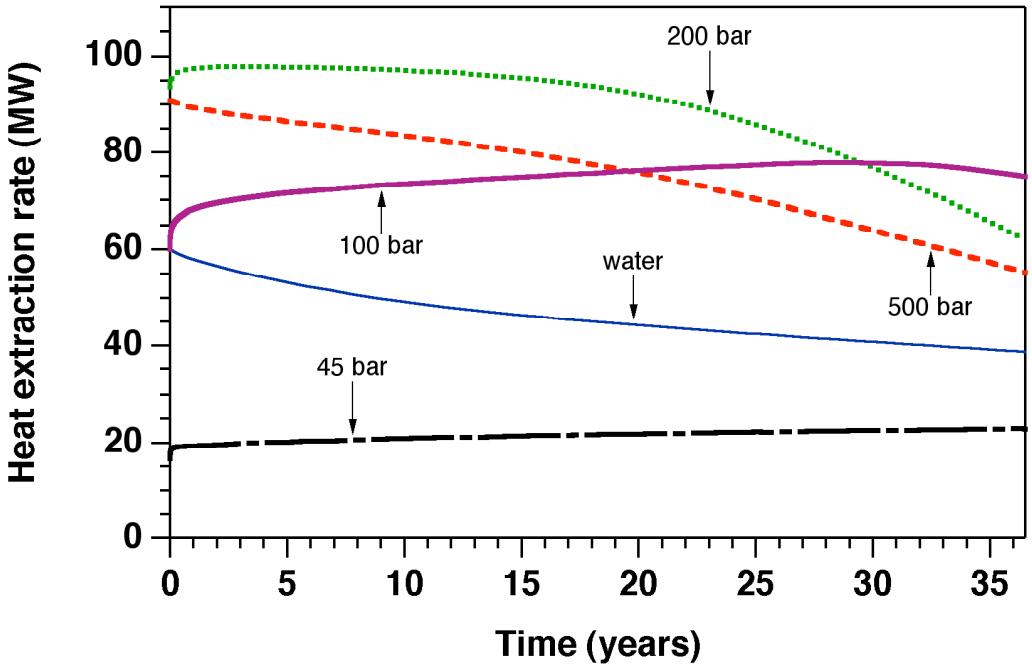

Figure 2. Simulated heat extraction rates (full well basis) for different reservoir pressures at T = 200 ^{o}C. The curve labeled "water" shows the production behavior of a water-based system, which is insensitive to reservoir pressure.

The time dependence of heat extraction rates when using CO_2 as working fluid shows some unusual features. For the 500 bar case there is a monotonic decline over time, in line with general expectations that, when injection and production pressures are held constant, heat extraction rates will decline over time as the reservoir heat inventory is being depleted. However, for a reservoir pressure of 200 bar heat extraction rates remain almost constant for the first 15 years, and for P = 100 bar there actually is a continuous increase over time up to 30 years, followed by a slow decline. This surprising behavior can be understood from the peculiar dependence of CO_2 mobility $m = \rho/\mu$ (density/viscosity) on temperature and pressure (Fig. 3). The heavy dashed lines in Fig. 3 indicate the range of thermodynamic conditions, from initial reservoir temperature of 200 ^{o}C to injection temperature of 20 ^{o}C, that will be encountered during fluid circulation. It is seen that at 500 bar pressure, declining reservoir temperatures will cause the mobility of CO_2 to decline also. This feature gives rise to the decline of mass flow rate over time for the 500 bar case (Fig. 4). For P = 200 bar reservoir pressure, fluid mobility increases as the reservoir is cooled from heat extraction, causing a continuous increase in mass production rates over time (Fig. 4). This almost compensates for the thermal depletion of the reservoir, causing heat extraction rates to remain nearly constant over an extended time period (Fig. 2). The eventual decline in heat extraction rates for P = 200 bar occurs when effects of thermal depletion become stronger than increases in mass production rate. For P = 100 bar, initial rates of heat extraction and mass flow are smaller than for P = 200 bar, due to smaller fluid mobility, but there is a strong increase in fluid mobility over time, when temperatures decline over part of the injector-producer flow path (Fig. 3). This causes heat extraction rates to increase, eventually surpassing those for the P = 200 bar case, due to less cumulative depletion.

The effects of temperature-dependent fluid mobility are further illustrated in Fig. 5, which shows pressure profiles along a line connecting injection and production wells for the 100 and 500 bar cases. For P = 500 bar, pressure gradients near the injection well (right hand side of Fig. 5) are considerably steeper than near the producer, consistent with the smaller fluid mobility at injection as compared to production temperature (Fig. 3). The opposite situation is encountered at P = 100 bar, leading to much larger pressure gradients near the producer as compared to the injector. The different nature of the pressure profiles is dramatized in Fig. 5 by plotting the P = 100 bar profile rotated by 180^{o}, which demonstrates the role reversal of pressure gradients near injector and producer by showing that the rotated profile for 100 bar is almost identical to the 500 bar profile.

It may be concluded that production behavior of EGS operated with CO_2 is much more sensitive to reservoir pressure than for water-based systems. Water mobility is dominated by viscosity effects, and decreases strongly with decreasing temperatures. In contrast, for CO_2 both density and viscosity depend significantly on temperatures, and do so in a manner that is different for different pressure regimes. This leads to strong mobility effects that may actually increase heat extraction rates over time for constant injection and production well pressures.

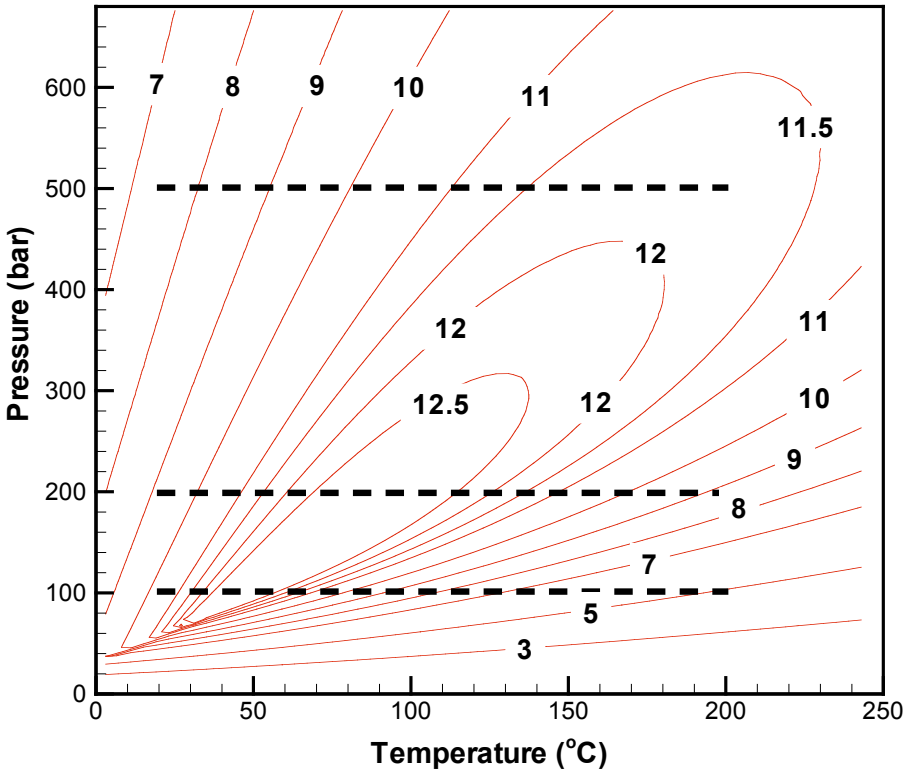

Figure 3. Mobility $m = \rho/\mu$ of CO_2 in units of 10^6 sm^{-2} as function of temperature and pressure. The heavy dashed lines indicate the range of thermodynamic conditions encountered at the different initial reservoir pressures.

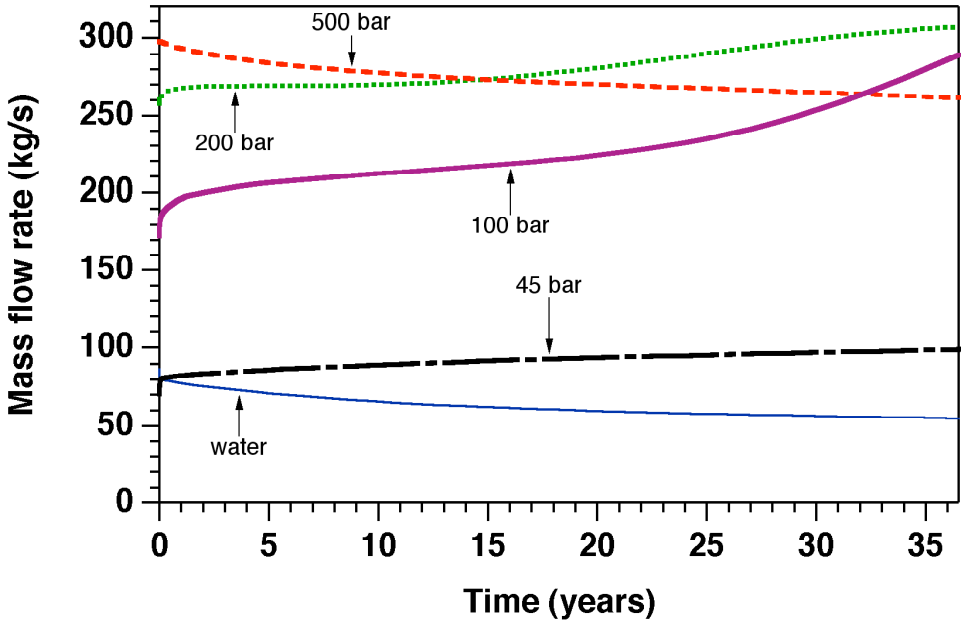

Figure 4. Simulated mass flow rates of CO_2-EGS (full well basis) for different reservoir pressures at T = 200 ^{o}C. The curve labeled "water" shows the production behavior of a water-based system, which is insensitive to reservoir pressure.

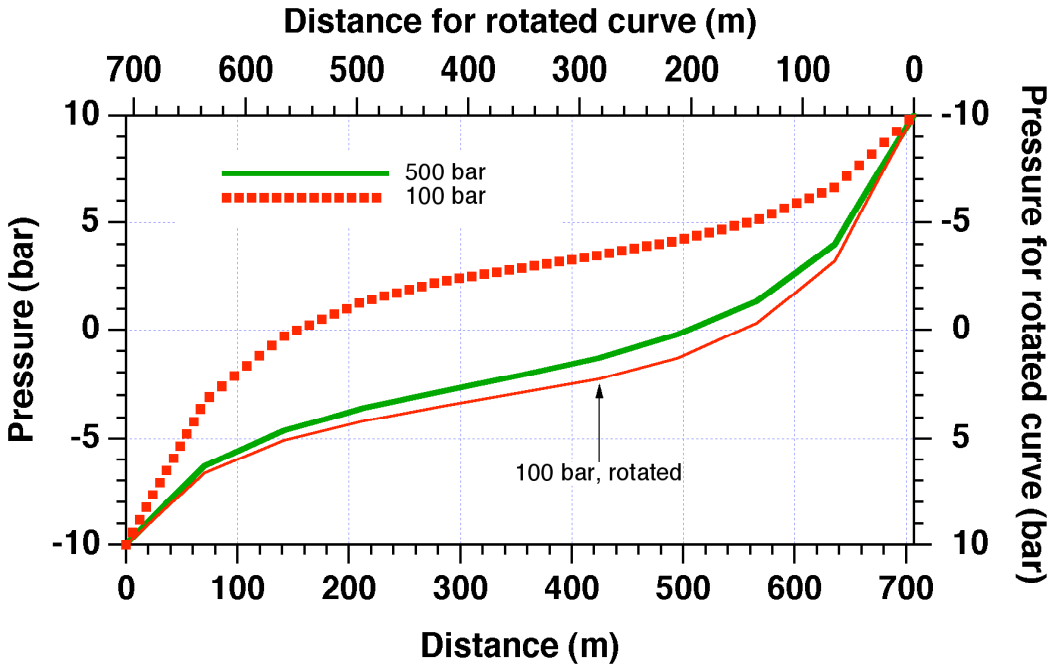

Figure 5. Pressure profiles for the P = 100 and 500 bar cases (CO_2-EGS) after 25 years of fluid circulation. Pressures are shown relative to original reservoir pressure. The production well is at a distance of 0, while the injector is at 707.1 m. For the P = 100 bar profile we also plot a curve that is rotated by 180^o, and is to be read with respect to the top and right axes.

Space Discretization Effects

The simulations performed above use a rather coarse space discretization. For the 1/8 of the five-spot modeled, our five-point parallel grid has 36 blocks (5x36 = 180 blocks after MINC discretization), and divides the injector-producer distance of 707.1 m into 10 grid increments of 70.71 m each. In an effort to examine the possible sensitivity of results to space discretization effects, additional calculations were performed for a 2-D areal grid with approximately half the grid spacing, having 144 blocks (5x144 = 720 blocks after MINC discretization) and a spatial resolution of 32.14 m. Simulated rates of mass flow and heat extraction for reservoir conditions

of (T, P) = (200 ^{o}C, 200 bar) for both CO_2 and water are shown in Fig. 6. Differences between the coarse and fine grids are surprisingly small.

It should be noted that for the same applied pressure differential between injector and producer, finer space discretization will reduce mass and heat flow rates, due to the fact that injection and production pressures are applied at smaller radii from the respective wells. In the fine grid calculations shown in Fig. 6 we compensate for this effect by increasing the injection-production pressure differential. The required correction is obtained by running a forced-isothermal water-only injection-production system to steady state. For the coarse (36 block) grid, this results in a steady water rate of 184.6 kg/s (full well basis), while for the fine grid (144 blocks), the steady water rate is 148.9 kg/s, a factor 0.807 smaller. We compensate for this by increasing the injector-producer pressure drop from 20 bar to (20/0.807) = 24.8 bar. Isothermal calculations for CO_2 using the coarse and fine grids, respectively, yield identical steady flow rates when applying this pressure correction. As expected and borne out by the results for non-isothermal calculations shown in Fig. 6, the pressure correction forces identical mass and heat rates at early times. As time goes on, minor discrepancies can be seen, but grid effects are small.

The weak sensitivity of fractured reservoir simulations to grid spacing has been noted previously [15]. It is explained by a compensation of space discretization errors between global flow through the fracture system, and local heat exchange between matrix blocks and fractures. Indeed, if the cold front emanating from the injection well advances too rapidly because of coarse space discretization, this will cause cooler conditions in the fractures downstream, and

will induce rates of heat transfer from the matrix blocks to increase, thus partially compensating for the lower temperatures.

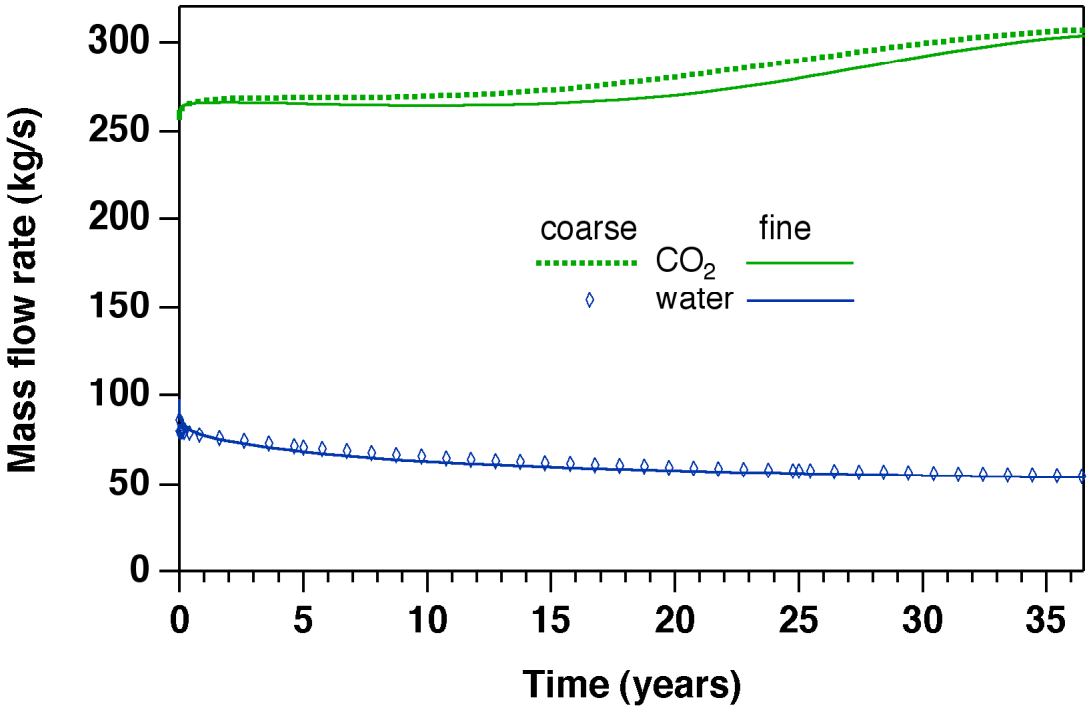

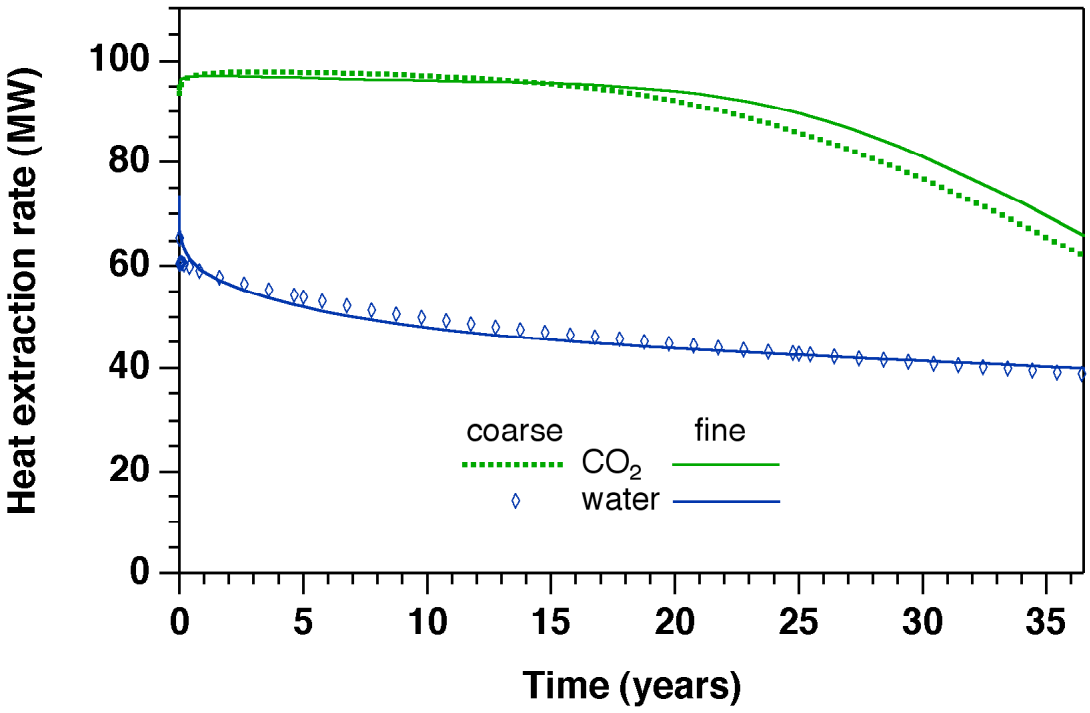

Figure 6. Comparison of mass flow (top) and heat extraction rates (bottom) for reservoir conditions of (T, P) = (200 ^{o}C, 200 bar) for both CO_2 and water for simulations using coarse and fine grids, respectively.

Three-dimensional Effects

The 2-D reservoir model discussed in the previous sections ignores effects of vertical flow, and does not account for a possible dependence of horizontal flow on depth. This will be a good approximation when net effects of gravity are weak, as is the case when fluid density varies only weakly with temperature and pressure. For example, for water the densities at injection and production conditions of (T, P) = (20 ^{o}C, 210 bar) and (200 ^{o}C, 190 bar) are 1007.6 and 877.5 kg/m^3, respectively [16], a difference of 14.8 %. For CO_2, however, densities at these conditions are 943.2 and 245.0 kg/m^3, respectively [17], a difference of 385 %! For CO_2 we may thus

expect very significant 3-D flow effects, as the denser fluid near the injection well flows not only horizontally, towards the producer, but also downward. Important 3-D effects may also arise from the dependence of the pressure differential between injection and production well with depth.

We performed a 3-D analysis of flow in EGS operated with CO_2, using the same reservoir properties (Table 2) and the same "coarse" grid of 1/8 of a five-spot as in the previous 2-D model, but in addition we discretized the reservoir thickness of 305 m into 6 layers, 5 x 50 m plus a 55 m thick layer at the bottom. The reservoir was initialized with supercritical CO_2 at T = 200 ^{o}C, and a vertical pressure equilibrium relative to P = 200 bar in the top reservoir layer. Fig. 7 shows the initial static pressure profile in the reservoir, along with static pressure profiles for injection (T = 20 ^{o}C) and production (T = 200 ^{o}C) wells, corresponding to fluid pressures of 210 and 190 bar, respectively, opposite the top reservoir layer. Although flowing pressure gradients will be less than static in injection wells, and greater than static in production wells, such differences are expected to amount to only a few percent, and fluid columns with static equilibrium provide a reasonable approximation for flowing pressures. Fig.7 shows that, due to the substantially larger fluid density at injection conditions, pressures increase with depth much more strongly at the injection than at the production side. Specifically, injection-production pressure differential increases with depth from (210 - 190) = 20 bar in the top layer to (233.5 – 196.2) = 37.3 bar in the bottom layer. Accordingly, an injection-production system with both wells open over the entire reservoir thickness will generate flow rates that substantially increase with depth. Thermal depletion of the reservoir will then be more rapid at greater depth, and

breakthrough of cold CO_2 at the production well may occur near the bottom at a time when substantial heat reserves remain near the reservoir top.

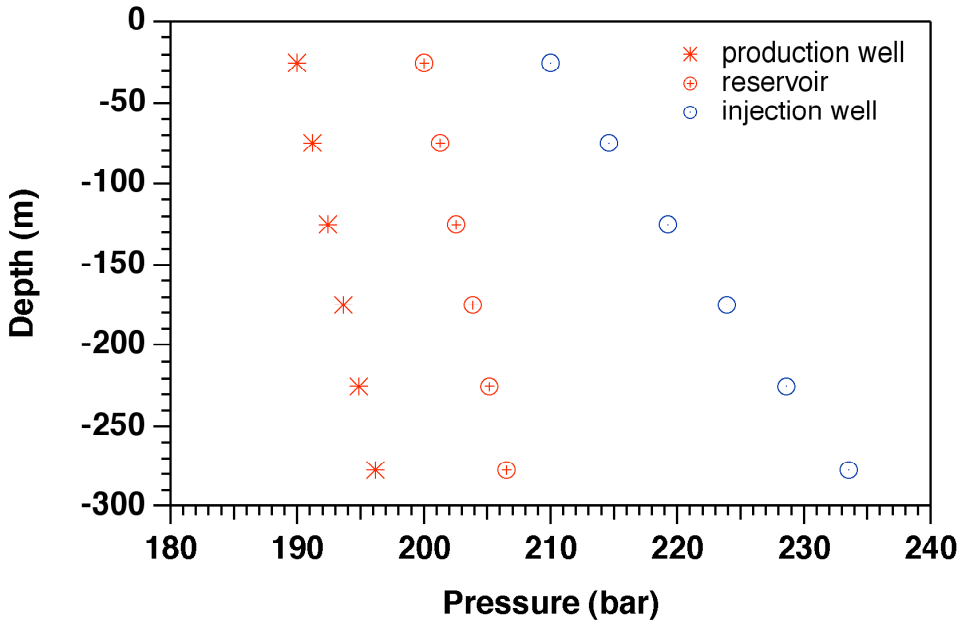

Figure 7. Static pressure profile in a reservoir of supercritical CO_2 at 200 ^{o}C, relative to a pressure of 200 bar in the top reservoir layer (25 m beneath reservoir top). Pressure profiles in production and injection wells are also shown, relative to production and injection well pressures of 190 and 210 bar, respectively. Temperatures are assumed as 200 ^{o}C for production, 20 ^{o}C for injection.

These expectations are borne out by results of numerical simulations. Fig. 8 shows flow rates into the different layers of the production well, and Fig. 9 shows the temperatures of the produced CO_2. Layer 6 (bottom) has the largest flow rates which show substantial increases over time, as parts of the reservoir cool and more cold dense fluid is diverted towards the bottom. The

large flows of cold fluid towards and along the reservoir bottom generate early thermal breakthrough, with significant decline in production temperature already after 5 years. In contrast, flows in layer 1 (top) are smallest, decrease over time, and take more than 25 years for significant temperature decline to occur. The strong increase in flow rates over time in layer 6 is in part due to a self-enhancement mechanism. Indeed, as the reservoir is cooled, fluid mobility

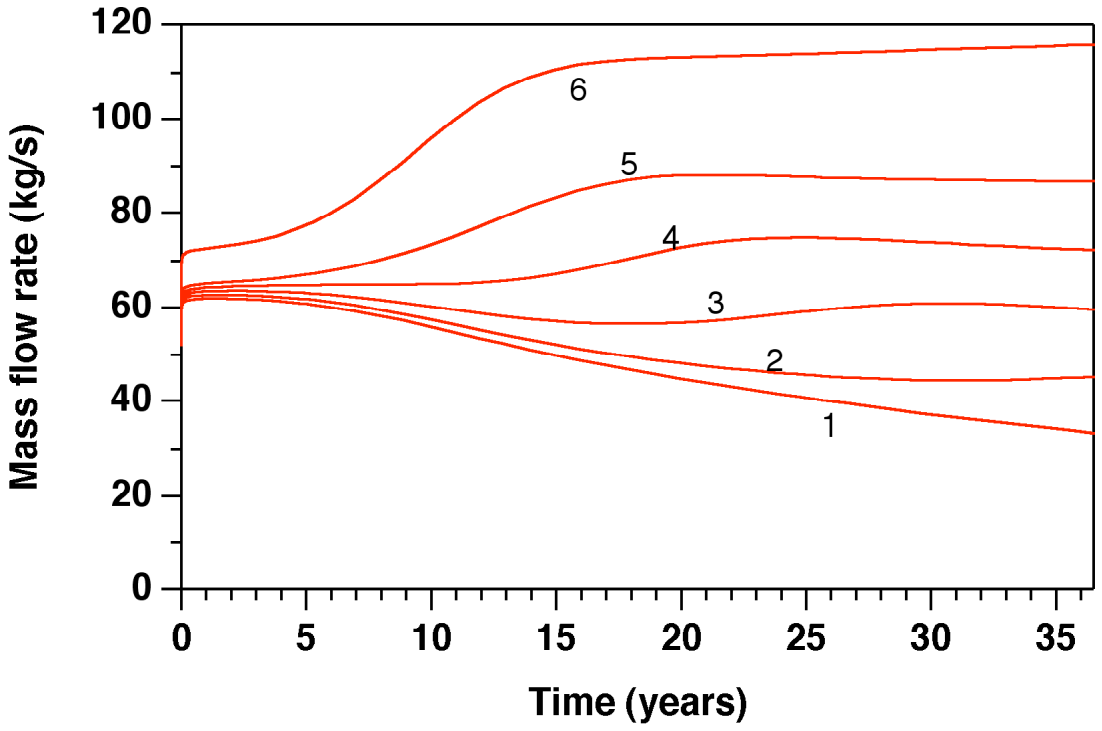

Figure 8. Production rates in the different reservoir layers (1 - top, 6 - bottom) for a CO_2-EGS with injection and production wells open in all layers.

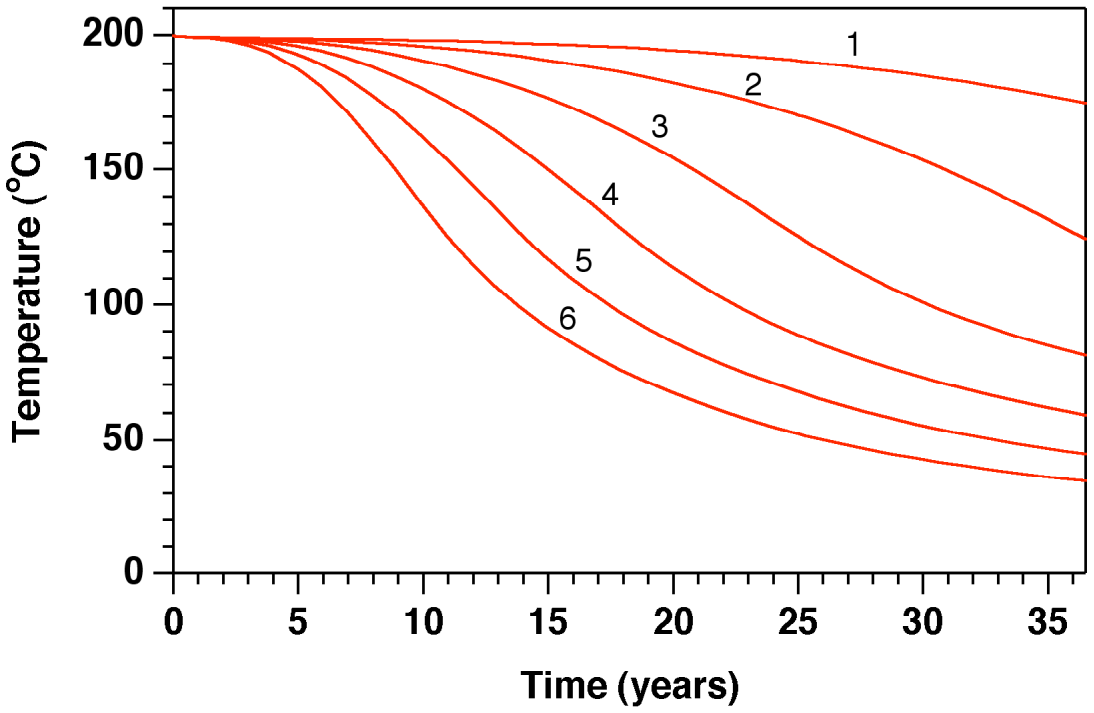

Figure 9. Production temperatures in the different reservoir layers (1 - top, 6 - bottom) for a CO_2-EGS with injection and production wells open in all layers.

increases (Fig. 3), providing a positive feedback between reservoir cooling and flow. The unfavorable heat extraction behavior observed when all reservoir layers are open in both injection and production well is evident from Fig. 10, which shows total net heat extraction and mass flow rates, summed over all layers of the production well. Heat extraction rates begin a significant decline after about 8 years, coincident with an increase in mass flow that is entirely due to inflow of colder fluid.

The mechanisms for early thermal breakthrough seen in the simulation just discussed suggest that an alternative scheme may be more favorable, in which the production well would be open only in the top layer(s) of the reservoir. This would avoid direct inflow of cold fluid at the bottom, lengthening the pathway for cold fluid and providing more opportunity for heat transfer from reservoir rocks. Fig. 11 shows net heat extraction and mass production rates for a scheme in which injection is made in all six layers, just as in the previous case, while the production well is open only in the topmost layer. It is seen that this indeed avoids early thermal breakthrough of injected fluid, leading to a nearly constant heat extraction rate for 25 years, followed by a slow decline that is a consequence of overall thermal depletion of the reservoir, not of premature thermal breakthrough.

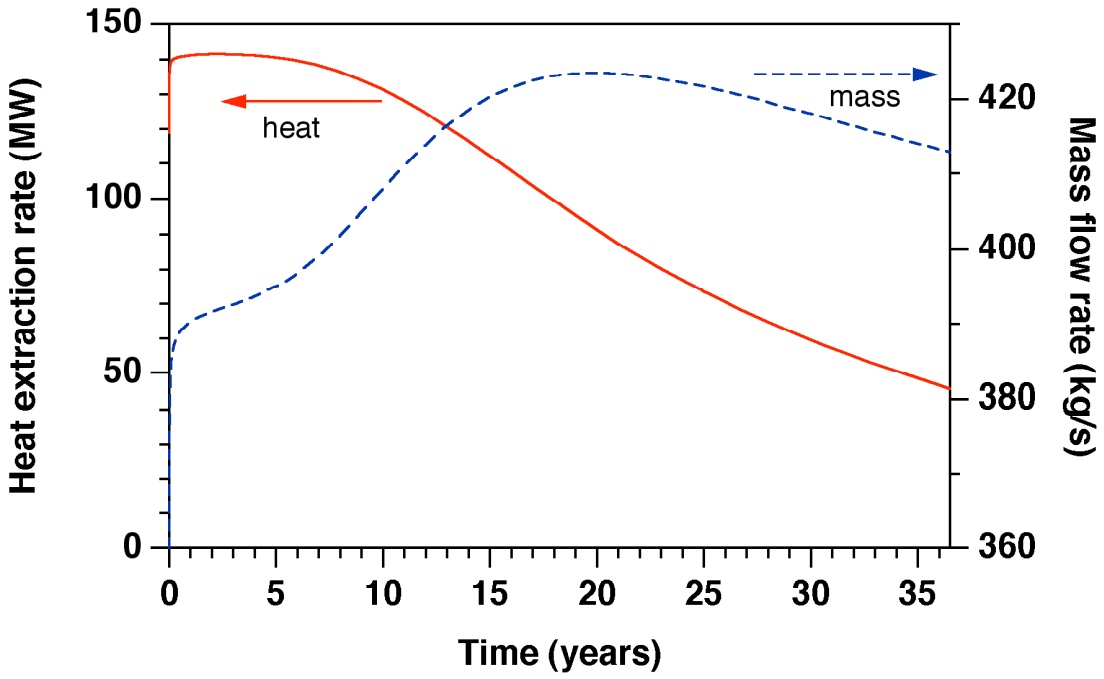

Figure 10. Total heat extraction and mass production rates from a CO_2 production well open in all six layers of a 200 ^oC reservoir.

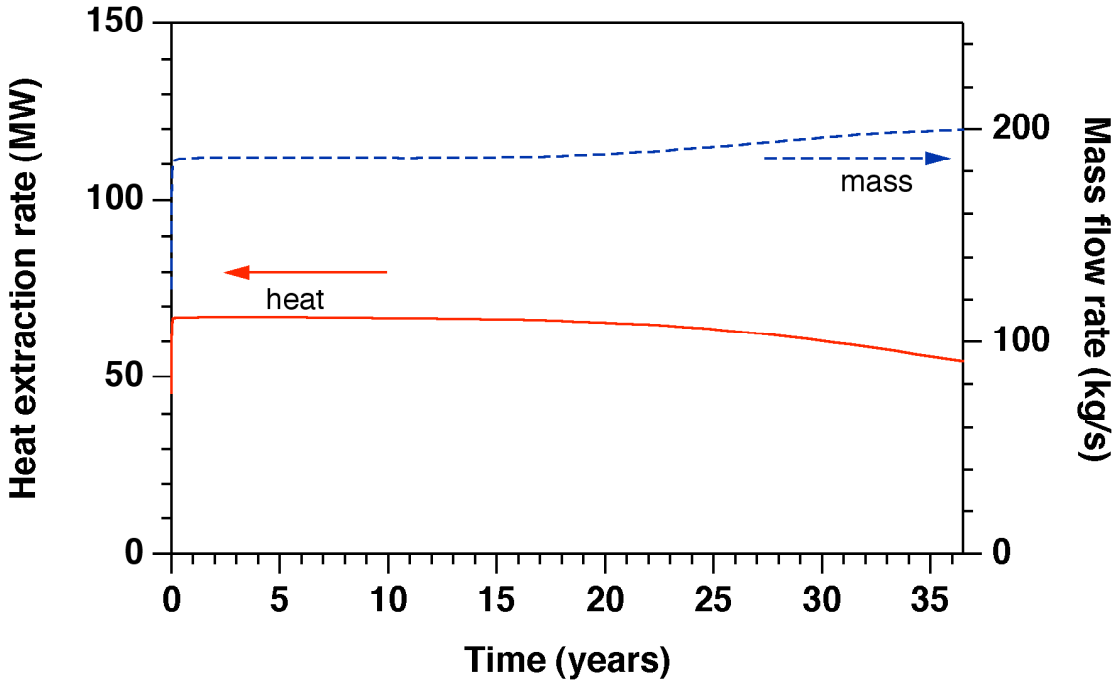

Figure 11. Heat extraction and mass production rates from a production well that is open only in the topmost 50 m thick interval of a 200 ^{o}C CO_2 reservoir.

Comparison with the 2-D case for (200 ^{o}C, 200 bar) shows smaller heat extraction and mass flow rates, due to the fact that the production well now is open in just 1 layer (50 m interval), whereas in the 2-D calculation it is open over the entire reservoir thickness (305 m). After 2 years of fluid circulation, rates of heat extraction and mass flow for 3-D are approximately stable at 67 MW and 195 kg/s, respectively, versus 95 MW and 270 kg/s for 2-D, indicating that both heat and mass rates are larger in 2-D by a factor of 1.44. In order to compensate for this factor, we performed another simulation for the 3-D system with the production well open only in layer 1, but with all permeabilities increased by a factor 1.44 to 72×10^{-15} m^2.

Of course, in an actual reservoir permeability is a given parameter, that could only be increased through hydraulic, thermal and/or chemical stimulation. Our purpose in evaluating a 3-D case with enhanced permeability is to force the same heat extraction and mass production rates as in 2-D at early time, and to then compare the longer-term depletion behavior to the 2-D case, as a means to obtain some measure of effective thermal sweep efficiency. We performed a similar problem variation for the 3-D system with injection into and production from all layers. For this system, early-time heat and mass extraction rates are a factor 1.45 larger than in 2-D, due to the substantial increase in the injection-production pressure differential with depth. Accordingly, for the system injecting into and producing from all layers, we conducted another 3-D run in which all permeabilities were reduced by a factor 1/1.45 = 0.69 to achieve the same early-time rates as in 2-D, so that longer-term thermal sweep efficiency again could be judged by comparison with the long-term decline seen in 2-D. The results are shown in Fig. 12. The 2-D approximation implies a perfectly uniform heat sweep in the vertical dimension, while the more rapid decline in heat extraction for 3-D reflects less favorable heat sweep, due to "gravity underride" of cold, dense fluid. Production from only the top reservoir layer (case 3-D A) gives less rapid decline than production from all reservoir layers (case 3-D B).

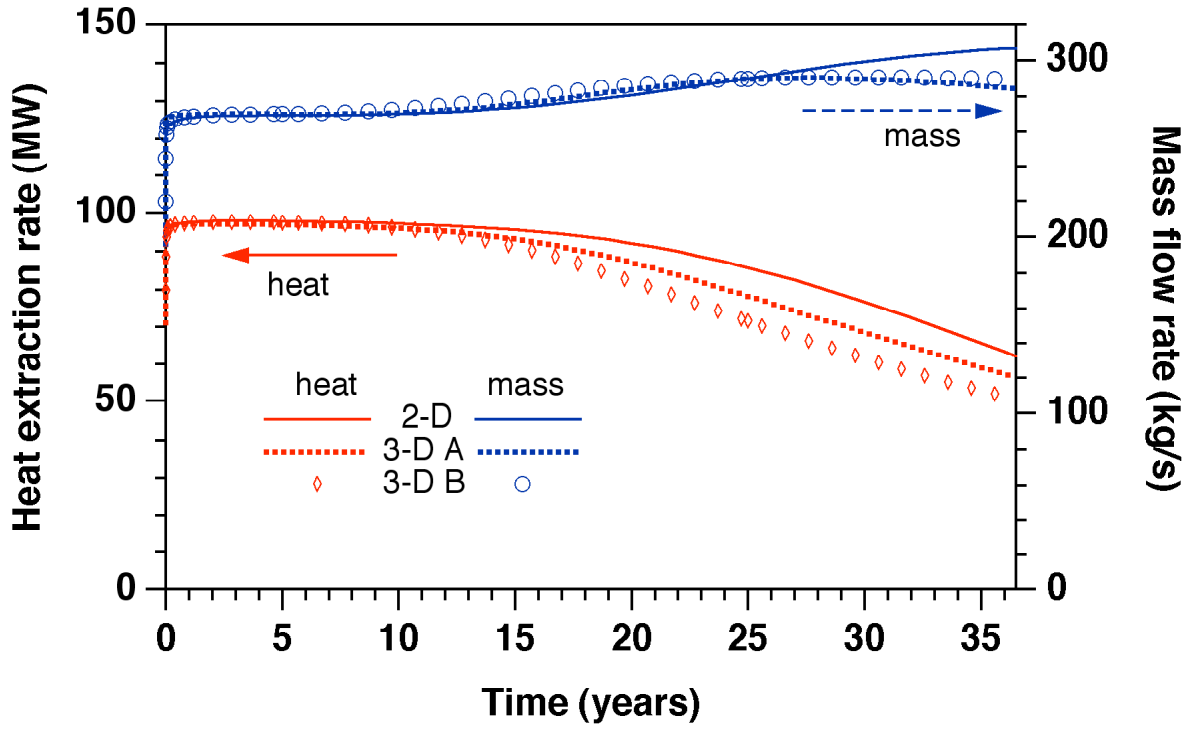

Figure 12. Heat extraction and mass production from differently operated 3-D system, compared with the 2-D system discussed previously. The curves labeled "3-D A" are for a system in which production is made only from the topmost 50 m interval, while "3-D B" is for a system in which the production well is open over the entire reservoir thickness of 305 m. Absolute permeabilities of the "3-D A" and "3-D B" systems were adjusted to achieve the same early-time heat and mass rates as in 2-D (see text).

Heat Transfer from Cap and Base Rocks

The simulations presented so far all assumed “no flow” (mass or heat) conditions at the top and bottom reservoir boundaries. However, even if the permeability of cap and base rocks is negligibly small, there would still be a possibility of conductive heat transfer to the EGS

reservoir as temperatures there decline from continued fluid circulation. A rough estimate of the importance of such heat exchange relative to local heat transfer from matrix blocks to the fractures in the permeable reservoir can be made from a consideration of geometric parameters. For the 1/8 of a five spot considered in our simulations, total interface area to cap and base rocks is 500 x 500 = 2.5×10^5 m^2, while reservoir volume is 500 x 250 x 305 = 38.125×10^6 m^3 (see Fig. 1). For cube-shaped matrix blocks with 50 m side length, the ratio of surface area to volume is 6 x 50 x 50/(50 x 50 x 50) = 0.12 m^{-1}, so that total matrix block surface area in the reservoir is 0.12 x 38.125×10^6 m^3 = 4.575×10^6 m^2. The combined interface area with cap and base rocks is thus a mere 5.5 % of the matrix block surface area. This suggests that conductive heat exchange with cap and base rocks will have minor significance initially, although it may increase in importance over time, as heat reserves within the reservoir are being depleted.

To further evaluate this issue, we have performed simulations with inclusion of cap and base rock heat exchange. This is accomplished by means of the semi-analytical technique developed by Vinsome and Westerveld [18], which models cap and base rocks as semi-infinite half spaces with initially uniform temperature, and represents the temperature profiles by means of a simple trial function, consisting of an exponential tail modified by a second-order polynomial, as follows.

$$T(x,t) - T_i = (T_f - T_i + px + qx^2) \exp(-x/d) \qquad (1)$$

Here x is the penetration depth into the conductive domain, t is time, T_i is initial temperature in the wall rock, T_f is the time-varying temperature at the wall rock boundary, and p and q are time-

varying fit parameters, that are determined from requirements of (1) energy conservation and (2) satisfying a diffusion (heat conduction) equation at the boundary. The p and q parameters will vary during the course of a simulation, and will be different for each grid block adjacent to cap and base rocks, depending on temperature changes in the flow domain. d is the penetration depth for heat conduction, given by

$$d = \sqrt{\Theta t}/2 \qquad (2)$$

where $\Theta = \lambda/\rho c$ is the thermal diffusivity, λ the thermal conductivity, ρ the density of the medium, and c the specific heat. For the parameters used here (Table 2) thermal diffusivity is $\Theta = 0.79 \times 10^{6}$ m^2/s. The method of Vinsome and Westerveld has been shown to give excellent accuracy; in a recent application that is relevant to this study it has been used to represent heat exchange between impermeable country rock and CO_2 escaping from a geologic storage reservoir along a fault zone [19].

As expected from the relatively small interface area for heat exchange, our simulations indeed showed that effects of cap and base rock heat exchange are small for the 2-D system, as well as for the 3-D system in which production is made only from a 50 m thick interval at the top of the reservoir. Somewhat larger although still modest effects are obtained in the 3-D system when production is made from the entire reservoir thickness. Heat transfer from the base rock slows the thermal decline at the bottom feed (layer 6; see Fig. 13), as well as providing larger heat extraction and mass flow rates (Fig. 14). Cap and base rock heat exchange would contribute more strongly and at earlier times if the reservoir were significantly thinner, or average fracture

spacing significantly larger than the 50 m assumed in our model, as this would increase the ratio of cap and base rock interface area to heat exchange area within the permeable reservoir.

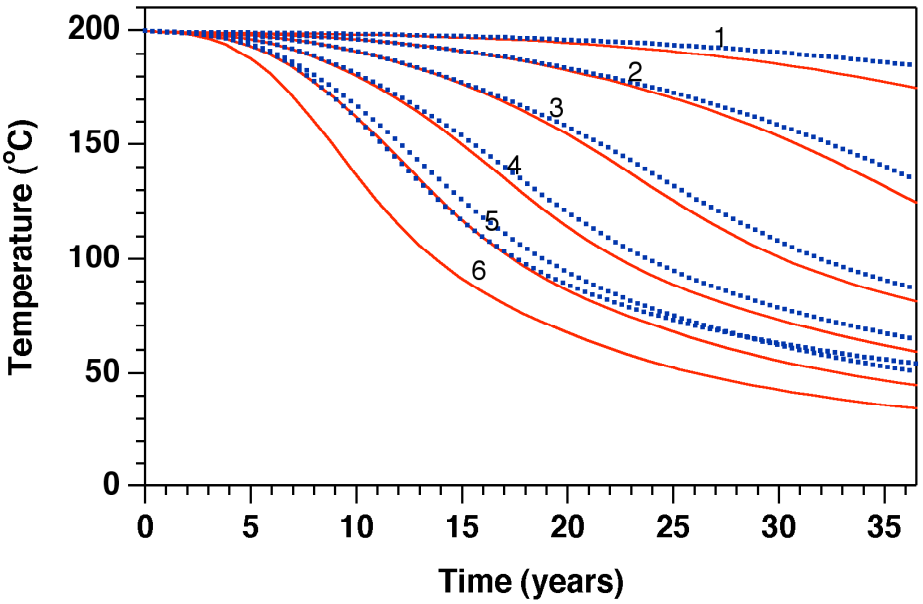

Figure 13. Production temperatures in the different reservoir layers (1 - top, 6 - bottom) for a CO_2-EGS with injection and production wells open in all layers. The thick dotted lines are for a system that includes heat exchange with cap and base rocks, while the thin solid lines are for a case in which such heat transfer is neglected.

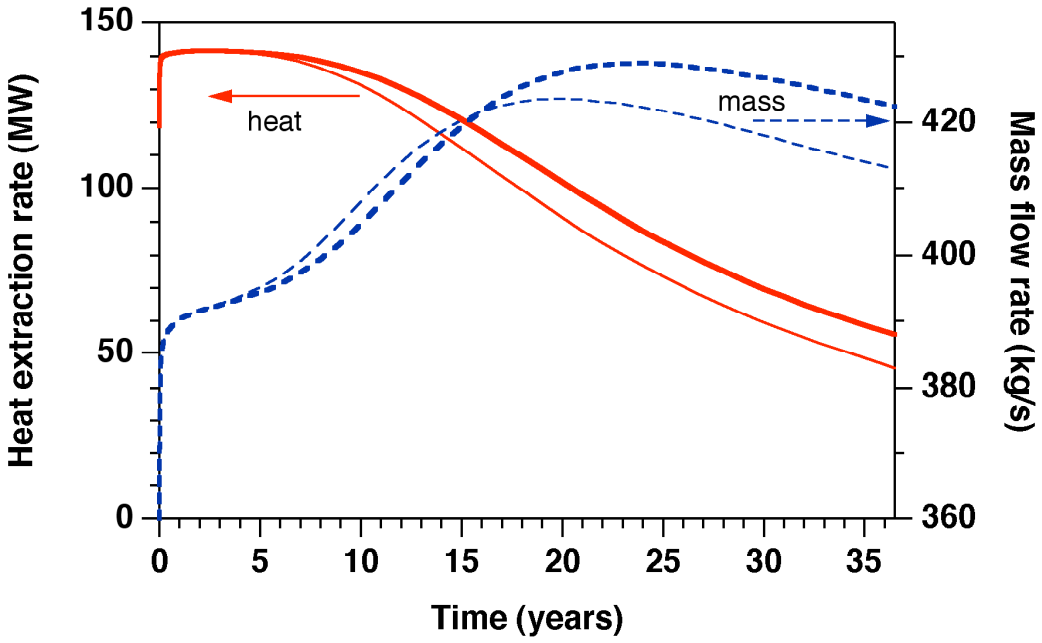

Figure 14. Total heat extraction and mass production rates from a CO_2 production well open in all six layers of a 200 ^oC reservoir. The thick lines are for a system that includes heat exchange with cap and base rocks, while the thin lines are for a case in which such heat transfer is neglected.

Concluding Remarks

Numerical simulation results presented in this paper confirm advantages of CO_2 over water as heat transmission fluid for enhanced geothermal systems (EGS), predicting larger energy extraction rates for CO_2 for the same applied pressures in injection and production wells. The mobility (= density/viscosity) of CO_2 depends in complicated fashion on both temperature and pressure, which gives rise to unusual features in the time dependence of mass flow and heat extraction rates. For certain reservoir pressures, heat extraction rates can actually increase for a time, due to strong increases in fluid mobility, even as the reservoir is being depleted thermally.

This paper has presented the first-ever three-dimensional simulations of injection/production behavior of EGS operated with CO_2. As expected from the much larger thermal expansivity of CO_2 as compared to water, gravity effects were found to be strong and capable of inducing preferential flow of cold, dense injected fluid along the reservoir bottom, with premature thermal breakthrough. Our results suggest that CO_2 production wells should not be open in the entire interval in which injection is performed; instead, production wells should be open only in a limited vertical interval near the reservoir top, while injection may be performed over the entire reservoir thickness.

Studies performed so far have shown great promise for EGS operated with CO_2, but much work remains to further explore and assess this novel technology. The customary hydraulic stimulation of EGS using aqueous fluids will produce a water-based reservoir, although stimulation treatment using CO_2 may provide an attractive alternative [20]. Understanding how continuous CO_2 circulation can remove the water from the core of an EGS and produce a "dry" CO_2 reservoir is a very important task for future work. This requires an accurate representation of phase partitioning in the water-CO_2 system for the entire range of temperature conditions from injector to producer [21]. The geochemical issues arising in development and operation of CO_2-based EGS also need to be addressed. Much is known about geochemical interactions at geothermal temperatures that would be induced by aqueous solutions of CO_2, as would be present in the peripheral regions of a CO_2-EGS [22]. Studies of chemical reactions between dry supercritical CO_2 and mineral assemblages are emerging only recently [23, 24].

The present study has focused on the energy extraction aspects of EGS with CO_2. Future work must also address CO_2 losses, as well as the question whether CO_2 lost from the main reservoir will remain contained safely and securely, perhaps through a combination of dissolution in the aqueous phase and formation of solid carbonates of low solubility [8].

Acknowledgement

Thanks are due to Jens Birkholzer for a careful review of the manuscript and the suggestion of improvements. This work was supported by Contractor Supporting Research (CSR) funding from Berkeley Lab, provided by the Director, Office of Science, and by the Assistant Secretary for Energy Efficiency and Renewable Energy, Office of Geothermal Technologies, of the U.S. Department of Energy under Contract No. DE-AC02-05CH11231.

References

[1] Brown, D. A hot dry rock geothermal energy concept utilizing supercritical CO_2 instead of water, *Proceedings,* Twenty-Fifth Workshop on Geothermal Reservoir Engineering, pp. 233–238, Stanford University, January 2000.

[2] Abé H, Duchane DV, Parker RH, Kuriyagawa M. Present status and remaining problems of HDR/HWR system design, *Geothermics,* Vol. 28, pp. 573–590, 1999.

[3] Durst D. Geochemical modeling of the Soultz-sous-Forêts hot dry rock test site: coupled fluid-rock interaction to heat and fluid transport. PhD dissertation, Université de Neuchâtel, Switzerland, 2002.

[4] Bächler D. Coupled thermal-hydraulic-chemical modeling at the Soultz-sous-Forêts HDR reservoir (France). PhD dissertation, Swiss Federal Institute of Technology, Zurich, Switzerland, 2003.

[5] Xu T, Pruess K. Numerical simulation of injectivity effects of mineral scaling and clay swelling in a fractured geothermal reservoir, *Transactions,* Geothermal Resources Council, Vol. 28, pp. 269–276, 2004.

[6] Rabemanana V, Vuataz FD, Kohl T, André L. Simulation of mineral precipitation and dissolution in the 5-km deep enhanced geothermal reservoir at Soultz-sous-Forêts, France, *Proceedings, Paper 1637.pdf,* World Geothermal Congress 2005, Antalya, Turkey, 24-29 April 2005.

[7] Andre L, Rabemanana V, Vuataz FD. Influence of water-rock interactions on fracture permeability of the deep reservoir at Soultz-sous-Forets, France, *Geothermics,* Vol. 35, No. 5-6, pp. 507–531, 2006.

[8] Fouillac C, Sanjuan B, Gentier S, Czernichowski-Lauriol I. Could sequestration of CO_2 be combined with the development of enhanced geothermal systems?, paper presented at Third Annual Conference on Carbon Capture and Sequestration, Alexandria, VA, May 3-6, 2004.

[9] Pruess K. Enhanced geothermal systems (EGS) using CO_2 as working fluid – a novel approach for generating renewable energy with simultaneous sequestration of carbon, *Geothermics,* Vol. 35, pp. 351–367, 2006.

[10] Baria R, Michelet S, Baumgärtner J, Dyer B, Nicholls J, Hettkamp T, Teza D, Soma N, Asanuma H, Garnish J, Megel, T. Creation and mapping of 5000 m deep HDR/HFR reservoir to produce electricity, *Proceedings, Paper 1627.pdf,* World Geothermal Congress 2005, Antalya, Turkey, 24-29 April 2005.

[11] Dezayes C, Genter A, Hooijkaas, GR. Deep-seated geology and fracture system of the EGS Soultz reservoir (France) based on recent 5km depth boreholes, *Proceedings, Paper 1612.pdf,* World Geothermal Congress 2005, Antalya, Turkey, 24-29 April 2005.

[12] Pruess K, Narasimhan TN. A practical method for modeling fluid and heat flow in fractured porous media, *Soc. Pet. Eng. J.*, 25 (1), 14-26, February 1985.

[13] Pruess K. The TOUGH codes—a family of simulation tools for multiphase flow and transport processes in permeable media, *Vadose Zone J.,* Vol. 3, pp. 738 - 746, 2004a.

[14] Pruess K. Numerical simulation of CO_2 leakage from a geologic disposal reservoir, including transitions from super- to sub-critical conditions, and boiling of liquid CO_2, *Soc. Pet. Eng. J.,* pp. 237 - 248, June 2004b.

[15] Pruess K, Wu YS. A new semianalytical method for numerical simulation of fluid and heat flow in fractured reservoirs, *SPE Advanced Technology Series,* Vol. 1, No. 2, pp. 63-72, 1993.

[16] IFC (International Formulation Committee). *A formulation of the thermodynamic properties of ordinary water substance,* IFC Secretariat, Düsseldorf, Germany, 1967.

[17] Altunin VV. *Thermophysical properties of carbon dioxide,* Publishing House of Standards, 551 pp., Moscow, 1975 (in Russian).

[18] Vinsome PKW, Westerveld J. A simple method for predicting cap and base rock heat losses in thermal reservoir simulators, *J. Canadian Pet. Tech.*, Vol. 19, No. 3, pp. 87–90, July-September 1980.

[19] Pruess K. Numerical simulations show potential for strong non-isothermal effects during fluid leakage from a geologic disposal reservoir for CO_2, B. Faybishenko, P.A. Witherspoon and J. Gale (eds.), *Dynamics of Fluids and Transport in Fractured Rock,* Geophysical Monograph 162, pp. 81–89, American Geophysical Union, Washington, DC, 2005.

[20] Mazza RL. Liquid-free CO_2/sand stimulations: an overview, paper SPE-72383, presented at the *Eastern Regional Meeting of the Society of Petroleum Engineers,* Canton, OH, October 2001.

[21] Takenouchi S, Kennedy GC. The binary system H_2O-CO_2 at high temperatures and pressures, *Am. J. Sci.,* Vol. 262, pp. 1055–1074, 1964.

[22] Ueda A, Kato K, Ohsumi T, Yajima T, Ito H, Kaieda H, Metcalfe R, Takase H. Experimental studies of CO_2-rock interaction at elevated temperatures under hydrothermal conditions, *Geochemical Journal,* Vol. 39 (No. 5), pp. 417-425, 2005.

[23] Regnault O, Lagneau V, Catalette H, Schneider H. Étude expérimentale de la réactivité du CO2 supercritique vis-à-vis de phases minérales pures. Implications pour la séquestration géologique de CO2, *C. R. Geoscience,* Vol. 337, pp. 1331–1339, 2005.

[24] Jacquemet N. Durabilité des matériaux de puits pétroliers dans le cadre d'une séquestration géologique de dioxyde de carbone et d'hydrogène sulfuré, PhD Thesis, University Henri Poincare, Nancy, France, 2006.

Table 1. Comparing CO_2 and water as heat transmission fluids for EGS. Favorable properties are shown bold-faced.

fluid property	CO_2	water
chemistry	**not an ionic solvent; poor solvent for rock minerals**	powerful solvent for rock minerals: lots of potential for dissolution and precipitation
fluid circulation in wellbores	**large compressibility and expansivity** **==> more buoyancy, lower parasitic power consumption to maintain circulation**	small compressibility, moderate expansivity ==> less buoyancy; substantial power requirements for pumps to keep fluids circulating
ease of flow in reservoir	**lower viscosity**, lower density	higher viscosity, **higher density**
heat transmission	smaller specific heat	**larger specific heat**
fluid losses	**may earn credits for storing greenhouse gases**	costly, obstacle to reservoir development

Table 2. Parameters for five-spot fractured reservoir reference case.

Formation	
thickness	H = 305 m
fracture spacing	D = 50 m
permeable volume fraction	f = 2%
permeability	$k = 50.0 \times 10^{-15}$ m^2
porosity in permeable domain*	$\phi_f = 50\%$
rock grain density	$\rho_R = 2650$ kg/m^3
rock specific heat	$c_R = 1000$ J/kg/°C
rock thermal conductivity	$\lambda = 2.1$ W/m/°C
Initial Conditions	
reservoir fluid	all CO_2, or all water
temperature	$T_{in} = 200$ °C
pressure	$P_{in} = 45$ - 500 bar
Production/Injection	
pattern area (Fig. 1)	A = 1 km^2
injector-producer distance	L = 707.1 m
injection temperature	$T_{inj} = 20$ °C
injection pressure (downhole)	$P_{inj} = P_{in} + 10$ bar
production pressure (downhole)	$P_{pro} = P_{in} - 10$ bar

* we include some wall rock in the definition of the fracture domain